Textures and Microstructures, Vol. 34, pp. 205–216
Reprints available directly from the publisher
Photocopying permitted by license only

STUDY OF THE DEFORMATION MECHANISMS OF THE SUPERPLASTIC ALLOY Al–Li 2090 BY TEXTURE ANALYSIS

M. T. PÉREZ-PRADO*, M. C. CRISTINA, O. A. RUANO and G. GONZÁLEZ-DONCEL

Department of Physical Metallurgy, Centro Nacional de Investigaciones Metalúrgicas (CENIM), C.S.I.C. Avda. Gregorio del Amo, 8, 28023 Madrid, Spain

(Received 4 February 2000)

The deformation mechanisms of a superplastic Al–Li 2090 alloy have been investigated by means of texture analysis. It has been found that both crystallographic slip (CS) and grain boundary sliding (GBS) operate in response to the applied stress over a wide range of deformation conditions. This is in contrast to well-accepted creep models, which predict that only one mechanism should operate and that the transition from one mechanism to another is abrupt and takes place over a narrow range of deformation conditions. Additionally, according to geometric (Taylor-type) models of uniaxial deformation for CS, the ⟨110⟩, ⟨111⟩, or ⟨001⟩ fibers should appear when 4, 6, or 8 slip systems operate. Here, however, CS contributes to stabilize orientations belonging to the α and β fibers.

Keywords: Aluminium alloys; Superplasticity; Texture; Deformation mechanisms

1. INTRODUCTION

Much effort has been devoted to elucidate the microscopic deformation mechanisms underlying superplastic deformation of aluminum alloys (Edington *et al.*, 1976; Langdon, 1982; Sherby and Wadsworth, 1989; Kaibyshev, 1995; Nieh *et al.*, 1996; Zelin and Mukherjee, 1996).

* Address for correspondence: Department of Mechanical and Aerospace Engineering, University of California, San Diego, 9500 Gilman Drive, La Jolla, CA 92093-0411, USA.

Grain boundary sliding (GBS) has commonly been regarded as the main deformation mechanism responsible for superplasticity. However, several investigations based on texture analysis have emerged throughout this decade in which a prominent role of slip during superplastic deformation is reported (Melton *et al.*, 1974; Bricknell and Edington, 1979; Tsuzaki *et al.*, 1990; Qing *et al.*, 1992; Blackwell and Bate, 1993; Liu and Chakrabarti, 1996). A similar behavior has been recently observed by the present authors in Al-5%Ca-5%Zn when tested along the transverse direction (Pérez-Prado *et al.*, 1996; 1998). It is therefore likely that the significant role of slip during superplasticity is not an isolated observation but a more general phenomenon.

Texture analysis has proved to be a very valuable tool for the study of deformation mechanisms. GBS, involving random grain rotations, is commonly associated to a decrease in texture intensity whereas crystallographic slip (CS) leads to the stabilization and strengthening of particular orientations (Edington *et al.*, 1976).

In this work the texture changes that take place during deformation of the superplastic alloy 2090 within and outside the superplastic regime will be investigated with the aim of studying the operative deformation mechanisms under the different testing conditions.

2. EXPERIMENTAL PROCEDURE

A well known fine-grained superplastic aluminum–lithium alloy was used for this study: 2090. Its composition and microstructural characteristics are described in detail elsewhere (Martin, 1988). This alloy was thermomechanically processed in order to achieve a stable fine grain size and, hence, superplastic response under appropriate testing conditions.

Uniaxial testing along the rolling direction (RD) and transverse direction (TD) was performed under three different combinations of temperature and strain rate in order to study the evolution of the texture. The three different testing conditions chosen are: $T = 400°C/10^{-2}\,s^{-1}$, $T = 550°C/10^{-2}\,s^{-1}$, and $T = 530°C/10^{-3}\,s^{-1}$ (optimum superplastic conditions).

Texture measurements were carried out by means of the Schulz reflection method in the as-received and deformed samples at the outer

surfaces (zone I) and in the mid-layer (zone II). Sample preparation consisted on grinding on successively finer silicon carbide papers and final mechanical polishing with 1 μm diamond paste. Details of the diffractometer used and the analysis method are given elsewhere (Pérez-Prado *et al.*, 1997; 1998). The texture was represented by means of direct (111) pole figures The intensity levels used to plot the pole figures were: 1.0, 1.5, 2.0, 2.5, 3.0, 3.5, 4.0, 4.5, 5.0, 5.5, and 6.0. Inverse stereographic triangles where also used to show the location of the RD and the TD corresponding to the main texture components. The RD and the TD are parallel to the tensile axis during longitudinal and transverse tests, respectively. Therefore, the rotation of these two directions during longitudinal and transverse deformation gives valuable information regarding the operative microscopic deformation mechanisms.

3. RESULTS

The texture of the as-received 2090 alloy is represented in Figure 1 by means of (111) pole figures. The locations of the RD and TD

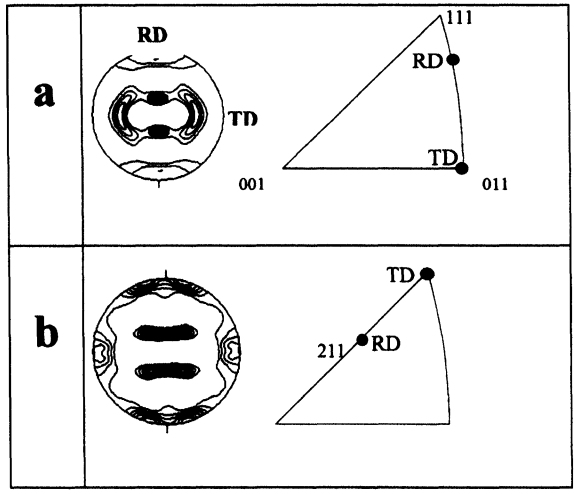

FIGURE 1 Texture ((111) pole figures and inverse stereographic triangles showing the location of the tensile axis) corresponding to the 2090 alloy in the as received state. (a) zone I (outer surface); (b) zone II (mid-layer).

corresponding to the main texture components have been plotted in inverse stereographic triangles. Figure 1(a) shows the texture of the outer surfaces of the sheet (from now on called zone I) and Figure 1(b) shows the texture of the mid-layer (from now on called zone II). It can clearly be seen that there is a through-thickness texture gradient in the rolled sheet: in zone I (Fig. 1(a)) the main component is $\{113\}\langle 332\rangle$ (close to Copper, or C), whereas in zone II (Fig. 1(b)) the main texture component is $\{011\}\langle 211\rangle$ (Brass or B). The RD in zone I is located along the $\langle 011\rangle$–$\langle 111\rangle$ boundary, 10° away from the $\langle 111\rangle$ pole. The TD is located at the $\langle 011\rangle$ pole. In zone II, however, RD is located along the $\langle 100\rangle$–$\langle 111\rangle$ boundary, at the $\langle 211\rangle$ pole. The TD is coincident with the $\langle 111\rangle$ direction.

The elongations to failure achieved after straining the 2090 alloy at $400°C/10^{-2}s^{-1}$, $550°C/10^{-2}s^{-1}$ and under optimum conditions for superplasticity ($530°C/10^{-3}s^{-1}$) along RD and TD are summarized in Table I. Already at 400°C moderate strains to failure (150%) are achieved. The strain to failure increases up to 250% at $550°C/10^{-2}s^{-1}$ and it reaches 560% when tested under optimum conditions for superplasticity. No significant differences in the elongations to failure during longitudinal and transverse tests were found.

The texture evolution observed in zone I of the 2090 alloy after deformation to failure at $400°C/10^{-2}s^{-1}$, $550°C/10^{-2}s^{-1}$ and under optimum conditions for superplasticity along RD and TD is illustrated in Figures 2(a)–(c) respectively. After longitudinal tests at 400°C and 550°C, the main component is the Copper (or C) component, $\{112\}\langle 111\rangle$. In both cases the crystallites rotate so that tensile axis shifts 10° along the $\langle 011\rangle$–$\langle 111\rangle$ boundary of the triangle, until it reaches the stable orientation $\langle 111\rangle$. After longitudinal tests under optimum conditions for superplasticity, however, the main texture component is

TABLE I Elongation (%) to failure corresponding to the 2090 alloy deformed along RD and TD under different conditions of temperature and strain rate

	RD	TD
$400°C/10^{-2}s^{-1}$	150	150
$550°C/10^{-2}s^{-1}$	300	250
Optimum conditions	560	560

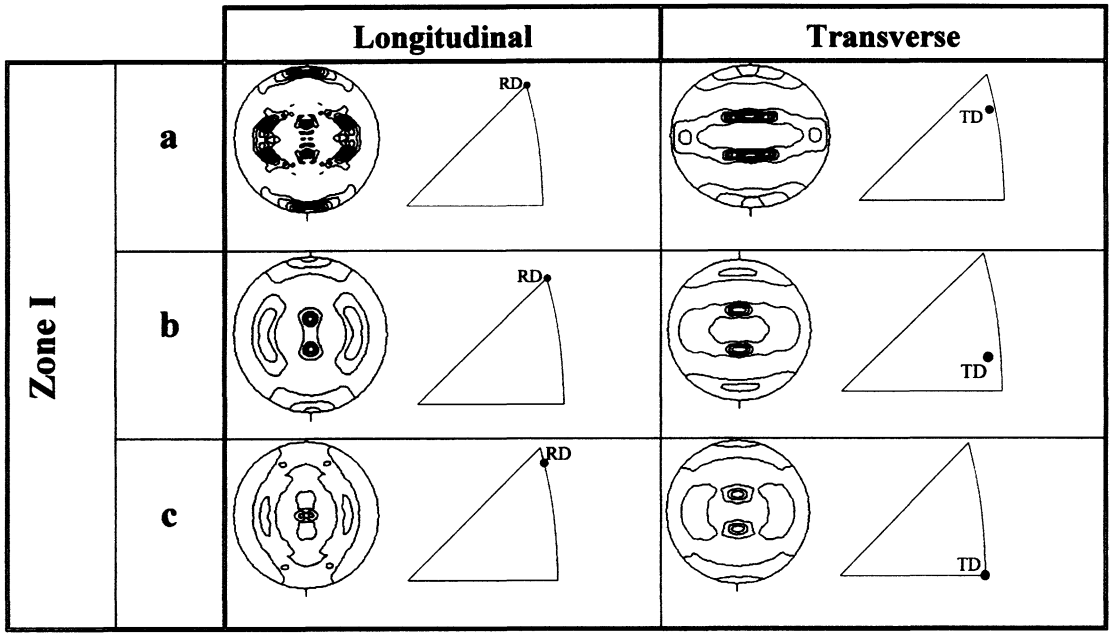

FIGURE 2 Texture ((111) pole figures and inverse stereographic triangles showing the location of the tensile axis) corresponding to zone I (outer surfaces) of the 2090 alloy deformed at (a) 400°C and $10^{-2}s^{-1}$, (b) 550°C and $10^{-2}s^{-1}$ and (c) optimum conditions for superplasticity along RD (longitudinal tests) and TD (transverse tests). The reference axes in the pole figures are the RD (vertical) and the TD (horizontal).

{225}⟨554⟩, only 5° apart from the Copper component. The rotation of the crystallites, in this case, is equivalent to a shift of the tensile axis of 5° along the ⟨011⟩–⟨111⟩ boundary towards the ⟨111⟩ direction, but without reaching it. In summary, small but distinctive changes in texture can be detected when testing along RD. The main component present in the as-received material, already initially close to the Copper component, rotates during deformation towards the exact Copper, which seems to be stable after tensile straining along RD.

After testing along TD, however, rather large rotations of the crystallites take place, leading to more dramatic texture changes. For the purpose of this work, it is more interesting to analyze the magnitude of the rotation than the specific texture components resulting after deformation. The latter will, thus, not be mentioned here. The rotation of the crystallites during deformation will be studied through the analysis of the corresponding rotation of the tensile axis in the inverse stereographic triangle (TD). Upon deformation at 400°C and 550°C, the tensile axis, initially parallel to the ⟨011⟩ pole, rotates along the ⟨011⟩–⟨111⟩ boundary of the stereographic triangle towards the ⟨111⟩ pole. After testing at 400°C the axis is located 10° away from the ⟨111⟩ direction, whereas at 550°C the tensile axis is located 20° away from ⟨111⟩. Upon deformation under highly superplastic conditions no rotation of the tensile axis was detected, and it remains stable in the ⟨011⟩ pole.

The results described above indicate that both CS and GBS are deformation mechanisms that operate simultaneously in response to the applied stress under all the testing conditions investigated. The predominance of one or the other depends on the particular testing conditions. The rotation of the tensile axis during deformation indicates the operation of CS. The amount of rotation may allow estimating the relative importance of CS under the different deformation conditions. On the other hand, the texture intensity gives a measure of the relative contribution of GBS (random grain rotation) to deformation, since GBS contributes to texture randomization. It can be seen that, after testing at 400°C, the rotation of the tensile axis is larger or equal than that observed under the two other testing conditions. Simultaneously, the texture intensity is high, even higher than that of the as-received material. Therefore a predominance of CS under this deformation conditions (400°C/10^{-2} s^{-1}) can be inferred. However, already at this

temperature moderately high elongations to failure were obtained (150%), that would not be achieved if CS were the only operative deformation mechanism. Upon deformation at 550°C the rotation of the tensile axis is equal or smaller than at 400°C and the intensity of the texture decreases, although still clearly defined texture components can be detected. This is consistent with the superplastic elongations to failure ($\sim$250–300%) achieved after testing at 550°C. The present results do not allow to determine whether CS or GBS predominates under these testing conditions. Finally, under highly superplastic deformation conditions, the texture intensity is weak and only slight rotations of the tensile axis could be detected in the longitudinal tests. Thus, GBS (random grain rotations) clearly predominates although CS must occur to some small extent.

Figure 3 illustrates the texture evolution in zone II of the 2090 alloy after testing at (a) 400°C and $10^{-2}\,s^{-1}$, (b) 550°C and $10^{-2}\,s^{-1}$ and (c) optimum conditions for superplasticity along RD and TD. During longitudinal tests at 400°C and 550°C, the tensile axis (RD) moves along the $\langle 100\rangle$–$\langle 111\rangle$ boundary of the triangle towards the $\langle 111\rangle$ pole. The rotation of the axis is larger after tests at the lowest temperature. However, after transverse tests at these two temperatures, the initial Brass texture remains stable during deformation. The tensile axis remains parallel to the $\langle 111\rangle$ direction. It can be clearly seen that the texture is sharper after testing at the lowest temperature (400°C), both along RD and TD. Under highly superplastic testing conditions a very weak texture was observed both after longitudinal and transverse tests.

The same arguments used to describe the deformation mechanisms predominant in zone I can be applied here. A very similar deformation behavior has been found in both zones. Again the results seem to indicate that both CS and GBS contribute to deformation in response to the applied stress. The rotation of the tensile axis is again larger after testing at 400°C than upon deformation under the other two testing conditions. Simultaneously, the texture intensity is higher at this low temperature. Therefore it can be concluded that CS predominates during deformation at 400°C/$10^{-2}\,s^{-1}$. During straining at 550°C the rotations of the tensile axis are smaller and the texture intensity weaker than at 400°C, but the texture is still clearly defined. Finally, the predominance of GBS under optimum superplastic deformation conditions is clearly evidenced by the dramatic decrease in texture intensity.

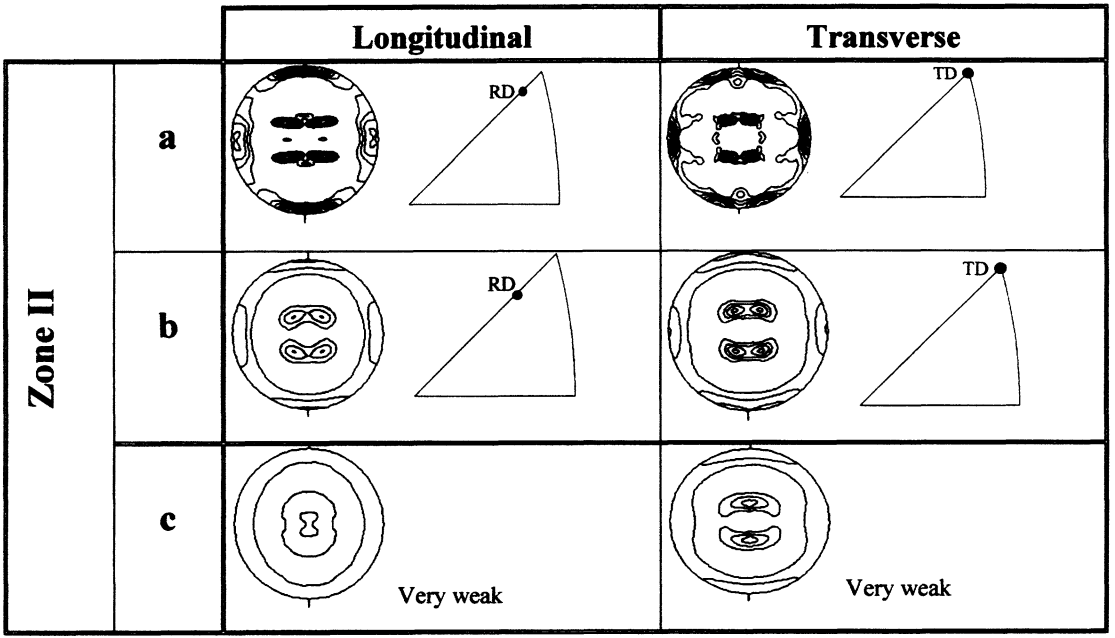

FIGURE 3 Texture ((111) pole figures and inverse stereographic triangles showing the location of the tensile axis) corresponding to zone II (mid-layer) of the 2090 alloy deformed at (a) 400°C and $10^{-2}s^{-1}$, (b) 550°C and $10^{-2}s^{-1}$ and (c) optimum conditions for superplasticity along RD (longitudinal tests) and TD (transverse tests). The reference axes in the pole figures are the RD (vertical) and the TD (horizontal).

4. DISCUSSION

The texture of this 2090 alloy, both in the outer surfaces and in the mid-layer, is well defined and is formed by orientations belonging to the α and β fibers in Euler space. This is a typical deformation texture predicted by Taylor-type deformation models for low rolling degrees (Hirsch and Lucke, 1988).

The present results suggest that there is a wide range of deformation conditions under which both CS and GBS contribute directly to deformation in this 2090 alloy. This is against well-accepted creep models (Chokshi *et al.*, 1993; Sherby and Wadsworth, 1989), according to which, firstly, only one deformation mechanism should operate and be rate-controlling during deformation at a given temperature and strain rate, and secondly, the transition from one mechanism to another should take place abruptly in a very narrow range of deformation conditions.

Additionally, the operation of CS during deformation leads to the stabilization of orientations belonging to the α and β fibers (the C, $\{112\}\langle 111\rangle$, orientation during longitudinal deformation and the B, $\{011\}\langle 211\rangle$, orientation during transverse deformation). This behavior is not consistent with geometric (Taylor-type) models for uniaxial deformation (Reid, 1973), according to which the operation of 4, 6, and 8 slip systems should give rise to the stabilization of the $\langle 011\rangle$, $\langle 111\rangle$, and $\langle 001\rangle$ fibers, respectively. The deformation of this 2090 alloy is characterized by the absence of fiber texture formation.

The deformation behavior of this Al–Li 2090 alloy, which does not conform to well-accepted creep models, has also been recently found in other similar superplastic alloys. Several investigators have reported the stabilization of α and β texture components during superplastic deformation (Melton *et al.*, 1974; Bricknell and Edington, 1979; Tsuzaki *et al.*, 1990; Qing *et al.*, 1992; Blackwell and Bate, 1993; Liu and Chakrabarti, 1996; Pérez-Prado *et al.*, 1996; 1997; 1998; Pérez-Prado and González-Doncel, 1999) as well as the apparent simultaneous operation of both CS and GBS during deformation (Melton *et al.*, 1974; Bricknell and Edington, 1979; Pérez-Prado *et al.*, 1996; 1997; 1998; Pérez-Prado and González-Doncel, 1999).

It is noteworthy that the superplastic materials in which this anomalous behavior has been observed, have well-defined as-processed

textures and undergo continuous recrystallization during the thermomechanical processing (TMP) or post-TMP annealing treatments. The process of continuous recrystallization is still not well understood but it is known that it takes place homogeneously in the microstructure and it contributes to the retention and sharpening of the texture (Humphreys, 1997). The geometric models for uniaxial deformation, however, usually assume a starting random texture. The presence of specific local grain arrangements, which is not contemplated in the classical deformation models, may thus deeply influence the deformation behavior of these alloys. This has already been demonstrated for rolling deformation by Hirsch (Hirsch, 1990), who showed that adjacent grains oriented as symmetric variants of the main texture components could undergo compatible plane strain deformation with the operation of only two slip systems.

5. CONCLUSIONS

The texture changes that take place during deformation of the superplastic aluminum-lithium alloy 2090 at three different testing conditions ($T = 400°C/10^{-2}\,s^{-1}$, $T = 550°C/10^{-2}\,s^{-1}$, and $T = 530°C/10^{-3}\,s^{-1}$ (optimum superplastic conditions)) have been investigated in order to study the main microscopic deformation mechanisms responsible for deformation. The main conclusions of this study are the following:

1. A through-thickness texture gradient is present in the as-received material. The as-processed texture is well-defined. In zone I (outer surfaces) the main component is $\{113\}\langle 332\rangle$ (close to Copper, or C), whereas in zone II (mid-layer) the main texture component is $\{011\}\langle 211\rangle$ (Brass or B). The main texture components belong to the α and β fibers.
2. Both CS and GBS contribute simultaneously and to different extents to deformation depending on the testing conditions. CS predominates at low temperatures, where only moderate elongations are achieved, and GBS predominates under optimum superplastic conditions.
3. CS contributes to stabilize orientations belonging to the α and β fibers. This is not consistent with current geometric models for uniaxial deformation, which predict the formation of the $\langle 011\rangle$,

⟨111⟩, and ⟨001⟩ fibers when 4, 6, and 8 slip systems operate, respectively.

4. The pattern of behavior described above seems to be common to several superplastic Al alloys that have well-defined starting textures and undergo continuous recrystallization during the TMP vand during post-TMP annealings.

Acknowledgements

MTP acknowledges an FPI grant from the Spanish Ministry of Education.

References

Blackwell, P. L. and Bate, P. S. (1993) The absence of relative grain translation during superplastic deformation of an Al–Li–Mg–Cu–Zr alloy. *Metallurgical Transactions A*, **24A**(5), 1085–1093.

Bricknell, R. H. and Edington, J. W. (1979) Textures in a superplastic Al-6Cu-0.3Zr alloy. *Acta Metallurgica*, **27**(8), 1303–1311.

Chokshi, A. H., Mukherjee, A. K. and Langdon, T. G. (1993) Superplasticity in advanced materials. *Materials Science & Engineering R*, **R10**(6), 237–274.

Edington, J. W., Melton, K. N. and Cutler, C. P. (1976) Superplasticity. *Progress in Materials Science*, **24**, 63–170.

Hirsch, J. and Lücke, K. (1988) Mechanism of deformation and development of rolling textures in polycrystalline FCC metals. II. Simulation and interpretation of experiments on the basis of Taylor-type theories. *Acta Metallurgica*, **36**, 2883–2904.

Hirsch, J. R. (1990) Correlation of deformation texture and microstructure. *Materials Science and Technology*, **6**, 1048–1057.

Humphreys, F. J. (1997) A unified theory of recovery, recrystallization and grain growth, based on the stability and growth of cellular microstructures. I. The basic model. *Acta Materialia*, **45**(10), 4231–4240.

Kaibyshev, O. A. (1995) Proc. Int. Conf. in Superplasticity: 60 years after Pearson (Edited by N. Ridley), The Institute of Materials, London. p. 25.

Langdon, T. G. (1982) The mechanical properties of superplastic materials. *Metallurgical Transactions A*, **13A**(5), 689–701.

Liu, J. and Chakrabarti, D. J. (1996) Grain structure and microtexture evolution during superplastic forming of a high strength Al–Zn–Mg–Cu alloy. *Acta Materialia*, **44**(12), 4647–4661.

Martin, J. W. (1988) Aluminum–lithium alloys. *Annual Review of Materials Science*, **18**, 101–119.

Melton, K. N., Edington, J. W., Kallend, J. S. and Cutler, C. P. (1974) Textures in superplastic Zn-40 wt% Al. *Acta Metallurgica*, **22**(2), 165–170.

Nieh, T. G., Wadsworth, J. and Sherby, O. D. (1996) *Superplasticity in Metals and Ceramics*, 1st edn. (Edited by D. R. Clarke S. Suresh and I. M. Ward), Cambridge University Press: Cambridge Solid State Science Series, 40–48.

Pérez-Prado, M. T., Cristina, M. C., Torralba, M., Ruano, O. A. and González-Doncel, G. (1996) Texture gradient evolution in Al-5%Ca-5%Zn sheet alloy after tensile superplastic deformation at high strain rate. *Scripta Materialia*, **35**, 1455–1460.

Pérez-Prado, M. T., Cristina, M. C., Ruano, O. A. and González-Doncel, G. (1997) Microstructural evolution of annealed Al-5 wt% Ca-5 wt% Zn sheet alloy. *Journal of Materials Science*, **32**(5), 1313–1318.

Pérez-Prado, M. T., Cristina, M. C., Ruano, O. A. and González-Doncel, G. (1998) GBS and Crystallographic slip during superplasticity of Al-5%Ca-5%Zn. *Materials Science and Engineering*, **244A**, 216–223.

Pérez-Prado, M. T. and González-Doncel, G. (2000) *Textures and Microstructures*, **34**(1).

Qing, L., Xiaoxu, H., Mei, Y. and Jinfeng, Y. (1992) On deformation-induced continuous recrystallization in a superplastic Al–Li–Cu–Mg–Zr alloy. *Acta Metallurgica et Materialia*, **40**(7), 1753–1762.

Reid, C. N. (1973) *Deformation Geometry For Materials Scientists*. Pergamon Press New York, 150–158.

Sherby, O. D. and Wadsworth, J. (1989) Superplasticity: Recent advances and future directions. *Progress in Materials Science*, **33**(3), 169–221.

Tsuzaki, K., Matsuyama, H., Nagao, M. and Maki, T. (1990) High-strain rate superplasticity and role of dynamic recrystallization in a superplastic duplex stainless steel. *Materials Transactions JIM*, **31**(11), 983–994.

Zelin, M. G. and Mukherjee, A. K. (1996) Geometrical aspects of superplastic flow. *Materials Science & Engineering A*, **208**(2), 210–225.